SILICON ISOTOPES IN GRANULITE XENOLITHS: INSIGHTS INTO ISOTOPIC FRACTIONATION DURING IGNEOUS PROCESSES AND THE COMPOSITION OF THE DEEP CONTINENTAL CRUST

Paul S. Savage[1#]*, R. Bastian Georg[2], Helen M. Williams[3] & Alex N. Halliday[1]

[1]Department of Earth Sciences, University of Oxford, South Parks Road, Oxford, OX1 3AN, UK

[#]now at: Department of Earth and Planetary Sciences, Washington University in St. Louis, One Brookings Drive, St. Louis, MO, USA. Tel: +1-(314)-935-5619 / Fax: +1-(314)-935-7361

[2]Water Quality Centre, Trent University, 1600 West Bank Drive, Peterborough, Ontario, K9J 7B8, Canada

[3]Department of Earth Sciences, Durham University, Science Labs, Durham DH1 3LE, UK

*corresponding author: savage@levee.wustl.edu

ABSTRACT

The silicon (Si) cycle is of great current interest but the isotopic composition of the continental crust has not been determined. Magmatic differentiation generates liquids with heavier Si and the lower crust, thought to be dominated by cumulates and restites, is predicted to have a light isotopic composition. This is borne out by the composition of many types of granite, which appear to have relative light Si for their silica content. Here we report the Si isotopic compositions of two granulite facies xenolith suites, from the Chudleigh and McBride volcanic provinces, Australia, providing new constraints on deep crustal processes and the average composition of the deep continental crust.

The xenoliths display a range of isotopic compositions (δ^{30}Si = -0.43 to -0.15 ‰) comparable to that measured previously for igneous rocks. The isotopic compositions of the McBride xenoliths reflect assimilation and fractional crystallisation (AFC), or partial melting processes. Silicon and O isotopes are correlated in the McBride suite and can be explained by AFC of various evolved parent melts. In contrast, the Chudleigh xenoliths have Si isotope compositions predominantly controlled by the specific mineralogy of individual cumulates. Using the xenolith data and a number of weighting methods, the Si isotope composition of the lower and middle crust are calculated to be δ^{30}Si = -0.29 ± 0.04 ‰ (95% s.e.) and -0.23 ± 0.04 ‰ (95% s.e.) respectively. These values are almost identical to the composition of the Bulk Silicate Earth, implying minimal isotope fractionation associated with continent formation and no light lower crustal reservoir.

Keywords: Silicon isotopes; lower continental crust; granulite xenoliths; igneous processes; AFC

41 # 1. INTRODUCTION

42

43 Silicon (Si) is the 2nd-most abundant element in the Earth's continental crust (Si ~28
44 wt.%; Rudnick and Gao, 2003) and is an important element in many geo- and biochemical
45 cycles (e.g. Tréguer et al., 1995, Basile-Doelsch, 2006). This "Si biosphere" is fed by
46 chemical weathering, which forms secondary minerals associated with large negative Si
47 isotope fractionation (Ziegler et al., 2005a&b; Opfergelt et al., 2012) and a complementary
48 heavy Si fluid phase (De la Rocha et al., 2000; Georg et al., 2009a). The exact Si isotopic
49 composition of the protolith itself, that is the continental crust, is not well constrained but this
50 can now be achieved with multi collector inductively-coupled-plasma mass-spectrometry
51 (MC-ICP-MS). These instruments have made it possible to precisely and accurately analyse
52 all three stable isotopes (^{28}Si, ^{29}Si and ^{30}Si) at high mass resolution (e.g. Georg et al., 2006).
53 Small isotopic variations generated through igneous processes are now detectable, and this in
54 turn, has permitted valuable and novel insights into how Si isotopes behave in high
55 temperature environments.

56 It is now known that the mantle is effectively homogeneous with respect to Si
57 isotopes. The resultant composition of the Bulk Silicate Earth (BSE) is well–defined (Savage
58 et al., 2010) with a value of $\delta^{30}Si$ = -0.29 ± 0.08‰ (2 s.d.), where
59 $\delta^{30}Si=[(^{30}Si/^{28}Si_{sample})/(^{30}Si/^{28}Si_{standard})-1]\times1000$. Magmatic differentiation of basalt results in
60 enrichment of the heavier isotopes in the evolved products (Fig. 1), with rhyolites having
61 $\delta^{30}Si$ of ~ -0.15 ‰ (Savage et al., 2011). This isotope fractionation appears predictable and
62 linked to SiO_2 as follows:

63 $$\delta^{30}Si\ (‰) = 0.0056 \times SiO_2\ (wt.\%) - 0.567\ (\pm 0.05;\ 2\ s.e.\ of\ the\ regression);$$

64 termed the "igneous array" for Si isotopes. Deviations from this array can be used as
65 evidence of sediment anatexis and assimilation, which is consistent with the composition of

66 many granites (Zambardi and Poitrasson, 2011; Savage et al., 2012). Surprisingly, this is not
67 just true of S-type granites; I-types also display a broad range of isotopic compositions for
68 their silica content unlike the products of differentiation or melting of juvenile basaltic crust.
69 Therefore, the deep crust from which silicic magmas are largely derived appears to be highly
70 heterogeneous with respect to Si isotopes, consistent with it being the site of protracted
71 geological processes that have introduced material from both surface and mantle reservoirs.
72 This paper tests this with the first high precision Si isotope data for samples of the
73 deep crust itself. This study also assesses (a) how cumulate formation and melt depletion
74 affect Si isotope composition, and (b) the average Si isotope composition of the deep
75 continental crust. If anything the average deep crust might be expected to be isotopically
76 light. This is because Si isotope fractionation relates to degree of polymerisation (Grant,
77 1954), wherein the least refractory, more Si-rich and, hence, isotopically heavier phases are
78 expected to be the first to melt, even though the presence of various "network-modifying"
79 cations such as Al can affect this relationship (e.g. Méheut et al., 2009). The Si isotope
80 composition of less Si-rich phases (clinopyroxene and olivine) is indeed isotopically lighter
81 than coexisting plagioclase (in samples from the Skaergaard Complex, Greenland; Fig. 1,
82 Savage et al., 2011). Deep continental crust includes, cumulate and restitic material as
83 significant components (Kempton and Harmon, 1992), which should bias the bulk
84 composition towards isotopically lighter compositions.
85
86 **2. SAMPLES FROM THE DEEP CONTINENTAL CRUST**
87
88 The continental crust can be split into three layers, upper, middle and lower, defined
89 on the basis of seismological profiles (e.g. Holbrook et al., 1992; Rudnick and Fountain,
90 1995) and examination of exhumed crustal sequences (e.g. Fountain and Salisbury, 1981;

Bohlen and Mezger, 1989). In general, these layers also correspond to changes in metamorphic facies, depending on temperature gradient. For an average crustal thickness of ~40 km, the upper continental crust (UCC) comprises the top 25 – 35% of the total crustal thickness (10-15km depth); this reservoir is composed predominantly of felsic granitoid material with significant sedimentary and metamorphic components. Below the UCC is the middle continental crust (MCC), comprising around 30 % of the total crustal thickness (between 10-15 km and 20-25 km depth) The MCC is composed of amphibolite and lower-granulite facies, predominantly andesitic meta-igneous and meta-sedimentary rocks. The lowest ~35% of the crust (below 20-25 km depth) the lower continental crust (LCC) is more primitive, consisting predominantly of granulite facies mafic meta-igneous rocks, with a minor but significant proportion of meta-sedimentary material (see Rudnick and Gao, 2003, and references therein). In the following, the MCC and LCC together will be described as the "deep continental crust".

Representative samples of the upper continental crust are readily available, such that the Si isotopic compositions of lithologies from this reservoir are comparatively well-studied (cf. Douthitt, 1982; Ding et al., 1996; Savage et al., 2012a&b). Samples of the MCC and LCC are more scarce than for the UCC, but they are available. In the main, two sample types have been utilised to investigate the composition of the deep crust. These are tectonically-exhumed high-grade metamorphic terranes (e.g. Bohlen and Mezger, 1989) and granulite facies xenoliths erupted through volcanic conduits (e.g. Dawson, 1977; Rudnick et al., 1986; Rudnick and Taylor, 1987; Condie and Selverstone, 1999; Villaseca et al., 1999; Liu et al., 2001). Many granulite facies xenoliths are of higher metamorphic grade and are thought to be derived from the LCC, whereas terranes, typically of amphibolite and lower granulite facies, are most likely representative of the MCC (Bohlen and Mezger, 1989).

In this study, we have chosen to analyse xenolith material as opposed to granulite

terrane samples, specifically a set of 16 granulite facies xenoliths, taken from the McBride and Chudleigh volcanic provinces, Queensland, Australia. This is because xenoliths are erupted relatively instantaneously from the deep crust, whereas terranes are typically exhumed over millions of years. This reduces the effect of retrograde metamorphism to negligible levels; only garnets appear to have undergone decompression reactions in the xenoliths which we have analysed (Rudnick et al., 1986; Rudnick and Taylor, 1987). It also limits the scope for any metasomatic processes that could affect Si elemental and isotopic composition.

The question as to how representative granulite facies xenoliths of the LCC is important to consider, as use of such material may bias estimates of the bulk Si isotopic composition of the deep crust. Specifically, felsic xenoliths may not survive transport in a magma hotter than their solidus. However, Rudnick and Fountain (1995) conclude that this should only happen if the crust was already partially molten before eruption. Even so, given the risk of bias, we have taken this into account in our calculations of crustal composition (Section 5.4).

2.1 McBride xenolith suite, Queensland, Australia

Eight granulite xenolith samples from the McBride volcanic province, northern Queensland, were analysed for Si isotopes. These samples were taken from a suite already well-characterised for major and trace elements, as well as radiogenic (Sr, Nd, U, Pb, Os) and stable (Li, O) isotopes (Rudnick and Taylor, 1987; Rudnick and Williams, 1987; Rudnick, 1990; Kempton and Harmon, 1992; Saal et al., 1998; Teng et al., 2008).

The McBride xenoliths used in this study were first described by Rudnick and Taylor (1987). The xenoliths are hosted in a single basaltic cinder cone of late Cenozoic age, are small (< 11 cm in diameter) and display a wide range of chemical and mineralogical contents,

with SiO_2 ranging from 41 to 67 wt.%. Thermobarometric techniques indicate that most of the xenoliths equilibrated in the lower continental crust (between 26 and 40 km), with only one sample, 85-107, displaying cooler temperatures indicative of a shallower (~18 km) origin. Equilibrium mineral assemblages suggest that minimal temperature and/or pressure variations have affected the samples since peak granulite metamorphism, and post-eruptive alteration is also limited. Strontium-neodymium isotope systematics suggests that the samples formed by mixing of a mantle-derived basaltic melt with pre-existing crustal material (possibly represented by the meta-sedimentary xenoliths) and subsequent magmatic differentiation (Rudnick, 1990).

The McBride xenoliths represent a range of protoliths, providing clear evidence for a chemically heterogeneous lower crust. Of the five mafic granulite facies xenoliths analysed in this study, two are “two pyroxene granulites”, representative of basaltic melts (85-100 and 85-120). The other three are garnet-clinopyroxene granulites, two of which are melt-depleted restites (83-159 and 85-114), the other a mafic cumulate (85-107). As well as mafic material, two felsic granulites (83-160 and 83-162) composed of quartz, garnet and K-feldspar (83-160 also has major plagioclase and orthopyroxene) were analysed. These have protoliths similar to the Phanerozoic calc-alkaline granitoid rocks present at the surface in the McBride volcanic province. Intermediate-composition granulite facies xenoliths from this suite are interpreted to have a sedimentary protolith; sample 83-157 is a metapelite composed of major plagioclase, garnet quartz and orthopyroxene. All sample and protolith information is taken from Rudnick and Taylor (1987).

2.2 Chudleigh xenolith suite, Queensland, Australia

To complement the McBride suite, eight granulite facies xenoliths were analysed from the Chudleigh volcanic province, northern Queensland, Australia. As with the above samples,

166 the Chudleigh xenoliths were taken from a suite already well-characterised for major and
167 trace elements as well as radiogenic (Sr, Nd, Pb, Os) and stable (O, Li) isotopes (Rudnick et
168 al., 1986; Rudnick and Goldstein., 1990; Kempton and Harmon., 1992; Saal et al., 1998;
169 Teng et al., 2008).

170 The Chudleigh xenoliths used in this study are described in detail by Rudnick et al.
171 (1986). They are hosted in Plio-pleistocene alkali basaltic vents, are large (between 5 and 50
172 cm), blocky and coarse-grained. Unlike the McBride xenoliths, these samples show little
173 variation in silica contents, ranging from 49 to 51 wt.%. All the samples are derived from
174 mafic igneous protoliths and display limited post-eruptive alteration.

175 Three types of xenolith are recognised in the Chudleigh suite (of which we have
176 analysed a representative selection): plagioclase-rich granulites (samples 83-107, 83-112, 83-
177 125, 83-127 and 83-131); pyroxene-rich granulites (samples 83-110 and 83-115) and
178 transitional granulites (which show chemical and mineralogical properties that lie between
179 the other two types; sample BC). Despite little variation in major element compositions, the
180 large mineralogical differences indicate a wide range of equilibration depths, between 20 and
181 40 km, and also large temperature differences of between 600 and 1000ºC (Rudnick and
182 Taylor, 1991). High Si/Na ratios in the samples provide evidence that the xenoliths are
183 unlikely to represent equilibrium melt compositions, instead, they are inferred to be igneous
184 cumulates, formed in a system where plagioclase was subordinate to ferromagnesian phases.
185 Sr-Nd systematics suggest that the cumulates and a coexisting melt phase (which is not
186 represented in the Chudleigh xenoliths) evolved through AFC processes (Assimilation and
187 Fractional Crystallisation; DePaolo, 1981), whereby mantle-derived basaltic melt assimilated
188 a pre-existing felsic crustal source and evolved through magmatic differentiation (Rudnick et
189 al., 1986).

190 These two sample suites will provide important insights into the behaviour of Si

isotopes in magmatic processes. First, the McBride suite, which is predominantly comprised of samples that represent equilibrium melt assemblages, can be used to confirm the robustness of the "igneous array" (Section 1), as these samples are not thought to be cogenetic. Second, the cumulate and restite samples from both the McBride and Chudleigh suites can help answer the important question as to whether these lithologies are consistently isotopically light (with respect to $\delta^{30}Si$), which will allows us to assess whether the deep continental crust is a thus far hidden isotopically light reservoir for silicon.

3. METHODS

Xenolith samples were provided in powder form by R. Rudnick. Although the samples were powdered in agate, this method has been shown to have no significant effect on the measured Si isotope composition of a sample (Savage et al., 2011, Zambardi and Poitrasson, 2011b). This should be true even for the smaller McBride xenoliths, as these are still large (~300g) compared to the amount of agate typically added to samples during milling (~0.10 % ≈ 0.3g; Allen, 1998). All samples and standards were processed for MC-ICP-MS analysis following the HF-free alkali fusion technique as detailed by Georg et al. (2006); such techniques have been utilised successfully by many research groups for Si isotope analysis and are comprehensively described elsewhere (e.g. Fitoussi et al., 2009; Zambardi and Poitrasson, 2011b; Savage et al., 2011, 2012a).

In brief: ~10 mg of sample powder was added to a silver crucible with ~200 mg of analytical grade NaOH flux (Merck) in pellet form. The crucible was heated to 720ºC for 12 minutes, removed and left to cool, then placed in ~20 ml of MQ-e (18.2 MΩ) water. After 24 hours, the fusion cake was transferred into solution, again in MQ-e water, and acidified to 1% v/v with HNO_3. Silicon concentrations were analysed using a spectrophotometer and fusion

yields were assessed. The average yield for this study was 100 ± 3 % (2 s.d.) for 16 fusions; no aliquot with a yield less than 97% was measured.

Sample solutions were purified before mass spectrometry using a single-pass column technique using BioRAD AG50W X12 200-400 mesh cation resin, and acidified to 1% v/v HNO_3 before analysis (Georg et al., 2006). There is no evidence for matrix effects from other anionic species on the measured Si isotopic ratios (Georg et al., 2006), and the external standards BHVO-2 and Diatomite were routinely analysed to assess method accuracy and reproducibility.

Isotopic measurements were made using a Nu Instruments Nu Plasma HR High Resolution Multi-Collector Inductively-Coupled-Plasma Mass Spectrometer (HR-MC-ICP-MS). Samples were aspirated using a 6 mm PFA concentric microflow nebuliser and desolvated using an Aridus II (Cetac, NE, USA). Isotopic analyses were made at "medium" resolution (resolving power $M/\Delta M \sim 3300$, where ΔM is defined at 5% and 95% for peak height; Weyer and Schwieters, 2003) to avoid poly-atomic interferences, which results in a ~ 85% reduction of instrument sensitivity. At sample Si concentrations of 750 ppb, a total signal of 1×10^{-10}A was typical.

Isotopic analyses were calculated via the standard-sample bracketing protocol, using NBS28 (NIST RM8546 silica sand) as the bracketing standard. Variations in Si isotopes are represented by the delta notation as $\delta^{30}Si$ or $\delta^{29}Si$, defined as the deviation in per mil (‰) of a sample's ratio of $^{x}Si/^{28}Si$ from the standard (NBS28), as such:

$$\delta^{30}Si = [(^{30}Si/^{28}Si_{sample})/(^{30}Si/^{28}Si_{standard}) - 1] \times 1000;$$

$$\delta^{29}Si = [(^{29}Si/^{28}Si_{sample})/(^{29}Si/^{28}Si_{standard}) - 1] \times 1000.$$

We discuss our Si isotopic data using $\delta^{30}Si$ values, which are roughly twice the magnitude of $\delta^{29}Si$ values. Assuming mass dependence, which is valid for terrestrial samples, this relationship was used as a further test for data quality.

4. RESULTS

4.1 External Standards

Sample data accuracy and precision were assessed using routine and repeated analysis of the external standards Diatomite and BHVO-2 during data acquisition. Diatomite is a natural pure silica standard (Reynolds et al., 2007; Georg et al., 2009b; Ziegler et al., 2010; Chakrabarti and Jacobsen, 2010; Armytage et al., 2011; Hughes et al., 2011; Savage et al., 2011, 2012a) and BHVO-2 is a USGS natural basaltic rock standard (Abraham et al., 2008; van den Boorn et al., 2009; Zambardi and Poitrasson, 2011b; Armytage et al., 2011; Savage et al., 2011, 2012a) that are both now widely utilised and well established in Si isotope studies. The Si isotopic data for 4 repeat runs of each standard (each on a different day) as well as the long term average, are given in Table 1. Our data for Diatomite (δ^{30}Si = 1.24 ± 0.07 ‰; 2 s.d., n = 4) and BHVO-2 (δ^{30}Si = -0.29 ± 0.05 ‰; 2 s.d., n = 4) agree well with other published values for the standards, and the calculated external precisions illustrate that sub-0.1‰ variations can be confidently resolved using our methods.

4.2 Granulite facies xenoliths

Silicon isotope data for the granulite facies xenoliths are given in Table 1 and plotted in Figure 1. Measurement uncertainty is given as both the 2 standard deviations (2 s.d.) and 95% standard error of the mean (95% s.e. = t × s.d./$(n)^{1/2}$, where t = inverse survival function of the Student's t-test at the 95% significance level and n-1 degrees of freedom).

The δ^{30}Si values for the xenoliths range from -0.43 to -0.15 ‰, with both suites displaying similar isotopic ranges (McBride δ^{30}Si = -0.40 to -0.15 ‰; Chudleigh δ^{30}Si = -0.43 to -0.20 ‰). These xenoliths, in particular the cumulate and restite lithologies, record

some of the lightest "high temperature" terrestrial Si isotope compositions so far measured with modern high precision techniques (Fig. 1). The range of data for the McBride suite (~0.25 ‰) is similar to that seen in other igneous settings where there is also a wide range of SiO_2 concentrations (i.e. Hekla; Savage et al., 2011). There is also a good correlation between $\delta^{30}Si$ and SiO_2 (R^2 = 0.81) for the McBride samples (Fig. 2). Significantly, the Chudleigh samples do not show a similar correlation, and the range of SiO_2 is much more limited; this is most likely because these samples are not representative of equilibrium melt assemblages (see Section 5.3).

5. DISCUSSION

5.1 Silicon behaviour during high-grade metamorphism

Before we can use the xenolith $\delta^{30}Si$ data to discuss Si isotope behaviour during igneous processes, we must first assess any effect that syn- and post-eruptive alteration and/or high-grade metamorphism may have had on the primary Si concentration and isotopic signatures of the samples.

Low-temperature processes such as chemical weathering and secondary mineral formation result in relatively large degrees of Si isotopic fractionation compared to that seen during igneous processes (e.g. Ziegler et al., 2005a&b; Georg et al., 2009b; Opfergelt et al., 2012), which enrich the product in the lighter isotopes (~1.0‰ negative enrichments are not uncommon in secondary phases). It is unlikely that such processes have altered the primary Si isotopic compositions of the samples, as all weathered surfaces were removed before analysis, and no clay minerals were identified (Rudnick et al., 1986; Rudnick and Taylor, 1987; Teng et al., 2008). Also, Li, which is more fluid-mobile than Si, shows no isotopic evidence that chemical weathering has affected the isotopic composition of the xenoliths

(Teng et al., 2008). The rapid exhumation of the xenolith material will have limited alteration during eruption and also minimised retrograde metamorphism (Section 2). Lastly, there is no evidence for magmatic infiltration into sample material (Rudnick et al., 1986; Rudnick and Taylor, 1987).

Xenolith material in a basaltic magma is not at equilibrium, so diffusion of material between xenolith and melt could modify the primary chemical composition recorded by the sample. Large variations measured in Li isotopes in the Chudleigh and McBride xenolith samples are attributed to kinetic isotope fractionation as a result of diffusion between xenolith and magma, or between minerals (Teng et al., 2008). This work identified two samples whose mineral δ^7Li values are equal to their bulk δ^7Li composition and are, therefore, in isotopic equilibrium; these samples (BC and 83-131 from Chudleigh) have δ^{30}Si values that encompass the Si isotopic range for the xenoliths ($\delta^{30}Si_{BC}$ = -0.40 ± 0.04 ‰, $\delta^{30}Si_{83\text{-}131}$ = -0.23 ± 0.04 ‰; Table 1). Given that Li isotopes are much more susceptible to kinetic isotope effects than Si (Richter et al., 2003, 2009; Huang et al., 2010), we are confident that kinetic processes have not affected the Si isotopic composition of the xenoliths.

Finally, we assess the effect that granulite facies metamorphism has had on the bulk Si isotopic compositions of the xenolith. In the presence of a volatile phase, Si mobility increases with increasing temperature and, under such conditions, is mobile during metamorphism. Prograde metamorphism to granulite facies often involves dehydration (e.g. Stähle et al., 1987), which will reduce concentrations of fluid-mobile elements (such as Cs, U, B etc; Rudnick et al., 1985; Leeman et al., 1992) and could therefore affect Si. There are some granulite terranes where metasomatism via high temperature CO_2-rich fluids has mobilised Si (Stähle et al., 1987; Newton, 1989) but in many of these cases this is related to retrograde metamorphism, which is avoided by studying xenoliths. Nevertheless, a major metasomatic event that significantly altered the silica content of a xenolith may also have

affected the primary $\delta^{30}Si$.

In fact, in the original studies on both xenoliths suites, no evidence of silica metasomatism was noted (Rudnick et al., 1986; Rudnick and Taylor, 1987); comparing the silica contents of the xenoliths to the average SiO_2 of their respective protoliths, as well as their metamorphic assemblages, there is no evidence that Si has been lost or gained to any significant degree during metamorphism and/or residence in the lower crust. This is strongly supported by the Si isotopic compositions; the $\delta^{30}Si$ of the McBride xenoliths correspond to the average isotopic composition of their inferred protoliths. Mafic melts have $\delta^{30}Si$ of -0.32 to -0.28 ‰, identical within error to the $\delta^{30}Si$ BSE value and MORB/IAB averages (Savage et al., 2010) and the felsic xenoliths have $\delta^{30}Si$ values of -0.22 to -0.15 ‰, which are within the range measured for dacites, rhyolites and I-type granites (Savage et al., 2011 – see Fig. 1).

Given that the xenoliths from Chudleigh and McBride appear to record their primary Si isotopic compositions, it is evident that some Si isotopic heterogeneity exists in the lower continental crust. Although not as variable as the upper crust (which reflects the effect of low-temperature weathering and biogenic processes; Savage et al., 2012b), the range of $\delta^{30}Si$ values in the deep continental crust is comparable to that displayed by igneous rocks of the oceanic and upper continental crust and mantle (Fitoussi et al., 2009; Savage et al., 2010, 2011, 2012a; Armytage et al, 2011). We will now focus on interpreting the Si isotope variations in each xenolith suite in turn.

5.2 Silicon isotopic variation in the McBride xenolith suite

The McBride xenolith suite consists of samples that are genetically unrelated, in that there are no obvious correlations with major or trace elements (Rudnick and Taylor, 1987), hence there is little risk of cogenetic bias. Also, the samples yield a wide spread of zircon ages, sampling lower crust that has formation ages spanning millions of years (between

341 Proterozoic and Permo-Triassic; Rudnick and Williams, 1987). Lastly, the wide range of
342 protolith lithologies represented by the McBride xenoliths contain most (if not all) of the rock
343 types that are thought to comprise the lower crust (e.g. Rudnick and Fountain, 1995).

344 As mentioned in Section 5.1, there are striking similarities between the Si isotopic
345 compositions of the melt-derived McBride xenoliths and those of their igneous counterparts
346 measured by previous studies. This is demonstrated by the strong positive correlation
347 between $\delta^{30}Si$ and SiO_2 (Fig. 2, $R^2 = 0.81$) which is collinear with the so-called "igneous
348 array" (see Section 1; Savage et al., 2011), also plotted in Figure 2 for comparison. The fact
349 that all of the meta-igneous xenolith data plot on or near to the "igneous array" is excellent
350 evidence that the processes that control the Si isotopic composition of igneous rocks erupted
351 at the surface are common to those controlling the composition of the lower crust; that is, the
352 relative Si-O bond strengths, (controlled predominantly by polymerisation degree and
353 chemical composition) between either a partial melt and restite, or a melt and crystallising
354 phase(s), fractionate Si isotopes because it is energetically more favourable for the heavier
355 isotopes to partition into phases with stronger Si-O bonds. This drives more silica-rich
356 samples to heavier Si isotopic compositions (e.g. Grant, 1954; Méheut et al., 2009; Savage et
357 al., 2011). This strong relationship also suggests that samples do not need to be cogenetic to
358 fall on the "igneous array"; rather, they simply need to represent equilibrium melt
359 compositions.

360 In detail, the mafic xenolith samples 85-100 and 85-120 have $\delta^{30}Si$ values (-0.32 to -
361 0.28 ‰); identical, within error, to those of MORB, IAB and mantle-derived suites (Savage
362 et al., 2010). These samples probably represent basaltic magma added to the lower crust by
363 underplating (Rudnick, 1990). Simplistically, the Si isotope composition of the majority of
364 the McBride samples can be explained by crystallisation of isotopically light olivine or
365 pyroxene (Fig. 1) from this basaltic material to generate a felsic melt with a heavy $\delta^{30}Si$

366 signature (samples 83-160 and 83-162), leaving a cumulate enriched in the lighter Si
367 isotopes. This is shown by a simple fractional crystallisation model in Figure 2, using the
368 average composition of the two mafic melt xenoliths as the starting composition (SiO_2 = 52
369 wt. %; $\delta^{30}Si$ = -0.30‰) and a bulk $\Delta^{30}Si_{solid\text{-}melt}$ value of -0.125‰ (as calculated for the
370 "igneous array" by Savage et al., 2011). The model fit to the xenolith data (and also the
371 igneous array) is good, and suggests that ~80% crystallisation is required to generate the
372 felsic melts, a plausible figure. Using mass balance (and assuming a closed system) the
373 cumulate compositions have been calculated for each 10% crystallisation step. The array of
374 compositions, also shown in Figure 2, is in broad agreement with the restite data. Although
375 these samples are not strictly cumulates, these isotopically light restites (samples 83-159 and
376 85-114) could be generated, by partial melting of a basaltic protolith, creating a isotopically
377 heavy feldspathic melt and a relatively light refractory restite. This is not to suggest that this
378 xenolith suite is cogenetic; rather the predictability of Si isotopes during magmatic
379 differentiation is such that even unrelated samples can be easily modelled using a single bulk
380 $\Delta^{30}Si_{solid\text{-}melt}$ value.

381 Although this simple framework can adequately explain the Si isotopic variation,
382 other isotope data indicate that petrogenesis of the McBride xenolith suite was not simply
383 closed-system magmatic differentiation. In particular, the Sr, Nd and O isotope compositions
384 of the xenolith suite do not lay within the ranges for mantle material (Fig. 3 & 4), suggesting
385 that a significant amount of assimilation of an evolved crustal source occurred during
386 petrogenesis (Rudnick, 1990; Kempton and Harmon, 1992). It is therefore pertinent to assess
387 whether assimilation may have altered the Si isotope composition of these xenoliths.

388

389 *5.2.1 $\delta^{30}Si$ vs. $^{87}Sr/^{86}Sr$*

390 No correlation exists between $\delta^{30}Si$ and initial (age corrected) $^{87}Sr/^{86}Sr$ and εNd (Fig.

391 3; Nd not shown). This is good evidence that assimilation of an isotopically evolved crustal
392 component has not resolvably affected the Si isotope composition of the xenoliths.

393 Previous work on the McBride xenoliths used AFC processes (assimilation and
394 fractional crystallisation) to explain the Sr and Nd isotopic variations (Rudnick, 1990). Here,
395 Sr and Nd isotope compositions were successfully modelled using an elevated r value (where
396 r is the ratio of assimilant flux to cumulate formation) of 0.9, and minor fractional
397 crystallisation (f = 0.9-0.95, where f is fraction of melt remaining). Figure 3 shows the r = 0.9
398 AFC trajectory in $\delta^{30}Si$ vs. $^{87}Sr/^{86}Sr$ space, calculated after DePaolo (1981), employing a
399 starting melt ("B") based on mantle-derived basalt ($\delta^{30}Si$ = -0.32‰) and assimilant based on
400 the composition of metasediment xenolith 83-157 ($\delta^{30}Si$ = -0.31‰; end member
401 compositions, D values and bulk $\Delta^{30}Si_{solid\text{-}melt}$ are given in Electronic Annexe EA-1). In this
402 case, AFC (r=0.9; f=0.95) successfully predicts the composition of the mafic xenoliths, but
403 fails to reach the heavier $\delta^{30}Si$ compositions of the felsic samples. This is because the meta-
404 sediment $\delta^{30}Si$ is unfractionated relative to the mafic melt.

405 One way to explain this is to invoke a separate AFC trend for the felsic samples, as
406 these xenoliths are not cogenetic. A good match to the data is returned using a much lower r
407 value (0.2) and larger melt depletion (~70%); however, such low r values are physically
408 unlikely for the hot lower crust, where rocks are already near melting (James, 1981). More
409 probable, the felsic samples can be easily explained via partial melting of a basaltic source,
410 which earlier formed along the AFC r=0.9 trend. Partial melting would fractionate $\delta^{30}Si$
411 parallel to the "igneous array" line in Figure 3 but would not affect $^{87}Sr/^{86}Sr$, resulting in a
412 melt enriched in ^{30}Si and leaving isotopically light restites.

413 A final possibility to consider is that the McBride xenoliths all derived from an
414 already enriched mantle (i.e., source rather than crustal contamination). This is demonstrated
415 by the two component mixing line in Figure 3, where between 20 and 40% contamination of

416 an isotopically enriched end member is required to explain the $^{87}Sr/^{86}Sr$ isotope compositions
417 of the xenoliths. However, this is unsupported by data from primitive basalts and mantle
418 xenoliths in the region, which indicate that the mantle below northern Queensland has a
419 primitive composition (Ewart et al., 1988).
420
421 *5.2.2 $\delta^{30}Si$ vs. $\delta^{18}O$*
422 Kempton and Harmon (1992) noted that O isotopes do not correlate well with
423 elemental or radiogenic isotope compositions in the McBride xenolith suite. This was
424 interpreted to be a result of the comparatively ancient pre-existing continental crust at this
425 locality, which, over geological time, has developed a variety of isotopically and elementally
426 heterogeneous crustal components. It is surprising then, that a plot of $\delta^{30}Si$ against $\delta^{18}O$ for
427 the McBride suite reveals a good correlation with O isotopes (Fig. 4).
428 Oxygen isotopes are fractionated by igneous processes to heavier compositions, but
429 not to the degree of isotope enrichment seen in the McBride suite (<1‰ variations between
430 basaltic and rhyolitic material are typical; Taylor and Sheppard, 1986). The oxygen isotope
431 data for the McBride samples are all at least 2.5‰ heavier than the canonical mantle value
432 ($\delta^{18}O$ = +5.5‰, Mattey et al., 1994), indicating the presence of a source that has been
433 affected by low temperature chemical weathering (e.g. Taylor and Sheppard, 1986). Even
434 though there is good evidence to suggest that Si isotopes have not been resolvably affected by
435 crustal contamination (due to the apparently unfractionated nature of the metasedimentary
436 material in this locality), the $\delta^{30}Si$ vs. $\delta^{18}O$ correlation merits comment, specifically: can we
437 model this relationship in terms of igneous processes?
438 As in Figure 3, we have attempted to model the data as a function of AFC processes.
439 Figure 4a shows a set of AFC trajectories in $\delta^{30}Si$ vs. $\delta^{18}O$ space, with a mantle-derived
440 starting melt identical to "B" in Figure 3 ($\delta^{30}Si$ = -0.32‰, $\delta^{18}O$ = +5.5‰). In this case, the

441 assimilant ("A") used in this model is dissimilar to that shown in Figure 3. This is because, as
442 noted by Rudnick (1990), the high degrees of assimilation of metasedimentary material
443 required by the isotope compositions of the McBride suite should be reflected in their major
444 elemental composition – which is not the case. To solve the assimilant problem, Kempton and
445 Harmon (1992) suggest that the contaminant is "mafic restite remaining from a
446 metasedimentary or $\delta^{18}O$-enriched metaigneous protolith after granite genesis," which could
447 be assimilated in large amounts without significantly altering the elemental composition of a
448 mafic melt. Hence, a putative restite was utilised as the assimilant, with a slightly lighter
449 $\delta^{30}Si$ than the metasediment (-0.37‰, averaged from the restite xenolith analyses), and the
450 most extreme $\delta^{18}O$ value (+13.2‰) measured from the McBride suite (see Electronic Annexe
451 EA-1).

452 As in Figure 3, the AFC (r=0.9, f=0.95) curve successfully predicts the more mafic
453 xenolith compositions, however, the felsic xenoliths cannot be explained by partial melting of
454 the mafic samples. This is show by the arrow in Figure 4a, which does not overlap the high
455 enriched O isotope composition of these samples. Although partial melting of material whose
456 source is modelled at lower f value (~0.85) along this curve could explain the O isotope data,
457 the melt would be too enriched in ^{87}Sr (see Fig. 3).

458 Also, in contrast to the $\delta^{30}Si$-$^{87}Sr/^{86}Sr$ data, an AFC trend with lower r (0.2) and high
459 melt depletion values does not pass through any of the data. This could indicate that the
460 composition of the assimilant is incorrect; however, assigning component "A" with a heavier
461 $\delta^{30}Si$ composition results in the model predicting the felsic samples but not the mafic
462 xenoliths – the same is found if the assimilant is assigned a much heavier O isotope
463 composition, using the r=0.2 curve. It appears, therefore, extremely difficult to modelling the
464 $\delta^{30}Si$ data $\delta^{18}O$ of the McBride xenoliths using AFC processes and a mantle-derived source.
465

A final adaptation of the model is to invoke that the starting melt was already ^{18}O-enriched before differentiation began. This could be generated a number of ways, either by source contamination resulting in an enriched mantle (although there is little evidence for this, see above), assimilation *without* fractional crystallisation of an evolved end-member (physically unlikely) or, similar to the "restite" model of granite genesis proposed by Chappell (e.g. Chappell et al, 1987), concomitant melting of a solid mixture of both primitive and evolved components. Nevertheless, a mixing line between a mantle-derived basalt and the restite contaminant (plotted in Figure 4b) gives a putative array of melt compositions; using the results from the model in Figure 3, we have used a mixture of 30% restite and 70% basalt as the starting melt ("M" in Fig. 4b; $\delta^{30}Si$ = -0.33, $\delta^{18}O$ = +8.0‰). Finally, AFC trends were calculated using "M" as the starting melt composition, again for different values of r. These models require r to be elevated, but values between 0.4 and 0.6, rather than 0.9, adequately explain both the Si and O isotope data for the McBride suite. These curves, all require high degrees of melt depletion (f = 0.2-0.4) in contrast to those of Rudnick (1990), although this may no longer be a problem given that the assimilant is mafic restite, rather than metasediment. On the basis of coupled $\delta^{30}Si$-$\delta^{18}O$ analyses, if appears that petrogenesis of the McBride xenoliths involved assimilation of an evolved crustal source into an already previously enriched, differentiating melt phase.

5.3 Silicon isotopic variation in the Chudleigh xenolith suite

In comparison to the variety of lithologies represented by the McBride suite, the Chudleigh xenoliths are all mafic cumulates (SiO_2 between 49.6 and 51.0 wt %), with isotopic compositions ranging in $\delta^{30}Si$ between -0.43 and -0.20 ‰. This is a much larger range than would be predicted if the Chudleigh xenolith protoliths represented mafic melts (see Fig. 2), so it seems likely that this large variation is a result of the cumulate-derived

mineralogy and composition of the xenoliths. Note that the Chudleigh xenoliths display much more mantle-like $\delta^{18}O$, $^{87}Sr/^{86}Sr$ and εNd (Fig. 3 and 4), indicating that crustal assimilation was either more limited than for the McBride samples, or that the crustal end-member was much less evolved.

In Section 1 we hypothesise that lower crustal igneous cumulates should have light Si isotope compositions relative to BSE, as a result of the enrichment of heavy Si isotopes in the melt phase during magmatic differentiation. In fact, only two cumulates are isotopically lighter than BSE, with the majority lying within the range of effusive igneous rocks, shown in Figure 1. The Chudleigh cumulates have significant modal abundances of plagioclase as well as olivine and pyroxene – plagioclase is typically isotopically heavier than BSE when forming from a mafic melt (Fig. 1), which would serve to balance out the lighter mafic phases.

This mineralogical control is demonstrated by a negative correlation between $\delta^{30}Si$ and Mg# (Mg# = molar $MgO/[MgO + 0.85 \times FeO_{total}]$; Fig. 5a; $R^2 = 0.63$, excluding sample 83-112 whose Mg# is much lower due to cumulate oxide phases, Rudnick et al., 1986). Furthermore, there is a positive correlation between $\delta^{30}Si$ and Eu/Eu* (Fig. 5b, $R^2 = 0.52$). Elevated Mg# can be an indication of large primary proportions of olivine and pyroxene (Mg-rich phases) and elevated Eu/Eu* (defined as $2\times Eu_N/[Sm_N\times Gd_N]^{0.5}$ where subscript N denotes that the concentrations are normalised to chondritic values) identifies the presence of cumulate plagioclase in a sample. Therefore, the Si isotopic composition of the Chudleigh xenoliths appear to be controlled by the ratio of olivine and pyroxene to plagioclase in the cumulate, with the most negative $\delta^{30}Si$ values corresponding to the largest proportions of Mg-rich phases. There is also a strong negative correlation between $\delta^{30}Si$ and CIPW normative diopside (not shown, $R^2 = 0.78$). Taken with the better correlation for Mg# than Eu/Eu*, this provides evidence that the abundance of ferromagnesian phases, more specifically pyroxene,

516 is the dominant control over Si isotopes in this cumulate system.

517 Using the Skaergaard mineral separate data (Fig. 1, Savage et al., 2011) and the CIPW
518 normative mineral compositions given in Rudnick et al. (1986), the predicted δ^{30}Si value of
519 the xenoliths can be calculated, assuming that the cumulates formed from a mafic melt. These
520 values are given as δ^{30}Si(m) in Table 1. While the range of predicted values (δ^{30}Si = -0.39 to -
521 0.24 ‰) is very close to the measured range, there is poor correspondence between the
522 predicted and actual isotopic composition for each xenolith sample. Either the fractionation
523 factors deduced from the mineral separate data are not universally applicable, or another
524 process, other than cumulate formation, may be affecting the Si composition of these
525 xenoliths.

526 Although the former cannot be discounted, major element characteristics provide
527 evidence for the latter. Rudnick et al. (1986) state that the variation in Mg# displayed by the
528 Chudleigh xenoliths is too large to be solely affected by the proportions of ferromagnesian
529 phases in the sample. They suggest that these data also reflect variations in the composition
530 of the coexisting melt; specifically, that those xenoliths with low Mg# have equilibrated with
531 a more evolved (Si-rich) melt. Assuming that a more Si-rich melt will have a heavier Si
532 isotopic composition, then cumulates deriving from this phase should be correspondingly
533 enriched in the heavier isotopes. This may be too simplistic, however, as the Si isotopic
534 composition of a mineral phase is likely to be controlled by the relative bonding
535 environments of Si between the phase and the melt (Méheut et al., 2009; Savage et al., 2011)
536 and an increase in the polymerisation degree of a melt will result in variations in the mineral-
537 melt fractionation factors. Nevertheless, the data provide evidence that the Si isotopic
538 compositions of the Chudleigh xenoliths are controlled predominantly by mineralogy, with
539 subtle isotopic variations introduced by compositional changes in the coexisting melt phase.
540 On the basis of these data, it appears that the lower continental crust is not a hidden light

541 reservoir for Si isotopes.

542

543 *5.4 Silicon isotopic composition of the lower and middle continental crust*

544 There are a number of ways with which the xenolith data can be used to calculate a Si
545 isotope composition for the LCC. The first is to take a simple arithmetic mean, which gives a
546 value of $\delta^{30}Si$ = -0.29 ± 0.15 ‰ (2 s.d.; Table 2); this value is identical to the canonical $\delta^{30}Si$
547 BSE value (Savage et al., 2010) and reflects the overall mafic composition of the this region,
548 and also that cumulates are not always enriched in the light Si isotopes, as was originally
549 suggested. The relatively large errors on the mean reflect the range of isotopic compositions
550 that are displayed in the lower crust. A second method is to take a weighted mean, using the
551 ratio of a sample's SiO_2 content against that of the LCC (53.4 wt.%, Rudnick and Gao, 2003)
552 as the weighting parameter. This gives a similar value, of $\delta^{30}Si$ = -0.28 ± 0.15 ‰ (2 s.d.;
553 Table 2), because most of the xenoliths analysed are also mafic.

554 The final way is more involved, and uses the average lithological compositions of the
555 LCC, as estimated by Rudnick and Fountain (1995), and average Si isotope compositions for
556 each lithology, to calculate a bulk estimate. This method is arguably the most robust, as bulk
557 xenolith composition and the lithologies represented vary considerably between continents
558 (e.g. Condie and Selverstone, 1999; Villaseca et al., 1999; Liu et al., 2001) and so using the
559 first two methods, rather than calculating a global average, could bias the calculation toward
560 the Australian lower crust.

561 This method starts by providing average values for the mafic, intermediate (andesitic),
562 felsic and sedimentary components of the crust. The felsic average was taken from the two
563 xenoliths that represent felsic melts from McBride, and the sedimentary average was taken
564 from measurements of shales and loess (Savage et al., 2012b). This estimate of $\delta^{30}Si$ = -0.32
565 ± 0.40 ‰ (2 s.d.) has large error bars, reflecting the broader range of data for sediments

566 compared to igneous rocks, although the mean value is very close to the one meta-sediment
567 analysed in this study (83-157). The mafic average is more complicated, because, as is shown
568 above, mafic cumulates have a much larger range of δ^{30}Si values than mafic melts – therefore
569 it is important to calculate a value that reflects the ratio of cumulate-derived to melt-derived
570 material in the lower crust. To estimate this, the global compilation of granulite facies
571 xenolith data of Kempton and Harmon (1992) was used to infer cumulate:melt:restite
572 populations; from this estimate, of the mafic xenoliths, 52% are melt-, 41% are cumulate-,
573 and 6% are restite-derived. This results in a mafic cumulate average of δ^{30}Si = -0.30 ±
574 0.07 ‰ (2 s.d.). Finally, the intermediate average is taken as the mean of the mafic and felsic
575 averages, viz. δ^{30}Si = -0.24 ± 0.16 ‰ (2 s.d.).

576 Table 2 shows the results for a number of different lower crustal types, with different
577 lithological proportions. There is very little variation between the calculated lower crustal
578 compositions, with all values (δ^{30}Si ranging from -0.30 to -0.26 ‰) close to the simple and
579 weighted means. The consistency of all of these values gives confidence that our original,
580 simple mean value of δ^{30}Si = -0.29 ± 0.15 ‰ (2 s.d.) is a good estimate of the Si isotope
581 composition of the lower crust. The precision on this estimate reflects the Si isotope
582 variability in the lower crust; however, the consistency of the average δ^{30}Si calculated using
583 various methods suggests that this value is better constrained than the precision indicates.
584 Using a 95% standard error reflects the precision of this mean at the 95% confidence level,
585 and gives a more precise estimate of δ^{30}Si = -0.29 ± 0.04 ‰ (95% s.e.). As an aside, the 2 s.d.
586 calculated using the various average δ^{30}Si lower crust compositions given in Table 2 is even
587 smaller (± 0.03 ‰).

588 Note that this value is identical to that of BSE (Savage et al., 2010). It was predicted
589 that, because mafic mineral phases have relatively light Si isotopic compositions, the process
590 of fractional crystallisation would create cumulate material with correspondingly light

591 compositions; therefore, the cumulate-dominated lower crust should also be isotopically light
592 relative to basalt and BSE. Here this hypothesis is disproven, as cumulate lithologies display
593 a wide range of Si isotope compositions, comparable to those of other igneous rocks (Fig. 1);
594 as such, the LCC has an isotopic composition that is more heterogeneous but almost identical
595 on average to the mantle.

596 The composition of the middle crust can also be estimated using the weighted mean
597 method and the lithological method as described above; these estimates are also presented in
598 Table 2. This method relies on some assumptions and a more robust estimate would make use
599 of Si isotope analyses of middle crustal lithologies (i.e. granulite and amphibolite facies
600 terranes), however, the exercise can give with a first order estimate. The weighted average
601 value for the middle crust is $\delta^{30}Si$ = -0.23 ± 0.15 ‰; 2 s.d. (± 0.04 ‰; 95% s.e.). This is
602 slightly heavier than both the lower and upper crust and reflects the predominantly andesitic
603 composition, and paucity of weathered sedimentary material, of this region.

604

605 **6. CONCLUSIONS**

606

607 Granulite xenolith samples from the Chudleigh and McBride volcanic provinces,
608 Australia, provide novel insights into how the Si isotope system behaves during igneous
609 processes, specifically cumulate formation and magmatic differentiation when crustal
610 assimilation is taking place. In addition, these samples also record the Si isotopic composition
611 of the deep continental crust.

612 Sixteen samples have been analysed, which display a range of isotopic data ($\delta^{30}Si$ = -
613 0.43 to -0.15 ‰) comparable to that measured elsewhere in igneous rocks, from the upper
614 crust, oceanic crust and mantle. For the McBride xenolith suite, magmatic differentiation
615 appears to be the major factor controlling Si isotope composition, whereby increasing SiO_2

616 content is accompanied by a concomitant increase in the heavier isotopes. This phenomenon
617 is observed globally, in many other magmatic systems (e.g. Savage et al., 2011). The
618 McBride data provides good evidence that samples do not need to be cogenetic for their Si
619 isotope compositions to exhibit this relationship; rather, they simply need to represent
620 equilibrium melt compositions, and therefore this relationship appears to be a fundamental
621 property of the Si isotope system.

622 Silicon isotope analysis has also provided insights into the petrogenesis of the
623 McBride xenoliths. On the basis of Si-Sr isotope systematics, petrogenesis of the McBride
624 xenoliths can be explained using a mantle-derived basaltic source that undergoes AFC to
625 form the mafic xenoliths; further partial melting of this material generates the felsic and
626 restite samples. This model does not, however, agree with the O isotope data; specifically, a
627 good correlation between $\delta^{30}Si$ and $\delta^{18}O$ is explained by AFC processes acting on a
628 previously-enriched source melt (relative to primitive mantle), containing ~30% of an
629 evolved component.

630 The cumulate-derived Chudleigh xenoliths have Si isotope compositions ranging from
631 $\delta^{30}Si$ = -0.43 to -0.20 ‰. Good relationships between $\delta^{30}Si$ and Mg#, Eu anomaly and CIPW
632 normative diopside content provide strong evidence that the Si isotope composition of these
633 samples is predominantly controlled by the mineralogy of individual cumulates. In particular,
634 phases that have higher Mg# tend to concentrate the lighter isotopes, therefore a cumulate
635 that is olivine or pyroxene-rich will have a lighter isotopic composition. The range of Si
636 isotope compositions in cumulates is similar to that displayed by effusive igneous material;
637 on this basis, the lower continental crust is not a hidden light reservoir for Si isotopes.

638 The average Si isotopic compositions of the lower and middle continental crust have
639 been calculated using the xenolith data, combined with a number of weighting methods. The
640 methods all give estimates that agree with one another, so we are confident that our

641 compositions are representative. These values are: $\delta^{30}Si = -0.29 \pm 0.04$ ‰ (95% s.e.) for the
642 LCC, and; $\delta^{30}Si = -0.23 \pm 0.04$ ‰ (95% s.e.) for the MCC. These values are almost identical
643 to the composition of the Bulk Silicate Earth, indicating that only minor isotopic fractionation
644 occurs as a result of continental crust formation.
645
646
647 *Acknowledgements:* The authors would like to thank Roberta Rudnick, who kindly provided
648 all the samples analysed in this study as well as reviewing an early version of this manuscript.
649 This work benefited immensely from scientific discussion with Ros Armytage, Julie Prytulak
650 and Kevin Burton. Expert editorial advice and incisive reviews and comments from three
651 anonymous reviewers and Mark Harrison greatly improved the manuscript. The authors
652 would also like to acknowledge the invaluable technical assistance and expertise provided by
653 Steve Wyatt, Nick Belshaw and Teo Krastev at the University of Oxford. This work was
654 funded by a NERC CASE studentship supported by Nu Instruments with additional analytical
655 costs by an ERC Advanced Fellowship to A.H.

656 **REFERENCES**

657 Abraham K., Opfergelt S., Fripiat F., Cavagna A., de Jong J. T. M., Foley S. F., André L. and
658 Cardinal D. (2008) δ^{30}Si and δ^{29}Si Determinations on USGS BHVO-1 and BHVO-2
659 Reference Materials with a New Configuration on a Nu Plasma Multi-Collector ICP-
660 MS. *Geostand. Geoanal. Res.* **32,** 193-202.

661 Allen M. A. (1998) Comminution of geological samples using Syalon based milling vessels:
662 comparison with established sample preparation methods. Anal. Commun. **35**, 75-78.

663 Armytage R. M. G., Georg R. B., Savage P. S., Williams H. M. and Halliday A. N. (2011)
664 Silicon isotopes in meteorites and planetary core formation. *Geochim. Cosmochim. Acta*
665 **75,** 3662-3676.

666 Basile-Doelsch I. (2006) Si stable isotopes in the Earth's surface: A review. *J. Geochem.*
667 *Explor.* **88,** 252-256.

668 Bohlen S. R. and Mezger K. (1989) Origin of granulite terranes and the formation of the
669 lowermost continental crust. *Science* **244,** 326-329.

670 Chakrabarti R. and Jacobsen S. B. (2010) Silicon isotopes in the inner Solar System:
671 Implications for core formation, solar nebular processes and partial melting. *Geochim.*
672 *Cosmochim. Acta* **74,** 6921-6933.

673 Chappell B. W., White A. J. R. and Wyborn D. (1987) The Importance of Residual Source
674 Material (Restite) in Granite Petrogenesis. *J. Petrol.* **28 (6)**, 111-1138.

675 Condie K. C. and Selverstone J. (1999) The crust of the Colorado Plateau: New views of an
676 old arc. *J. Geol.* **107,** 387-397.

677 Dawson J. B. (1977) Sub-cratonic crust and upper mantle models based on xenolith suites in
678 kimberlite and nephelinitic diatremes. *J. Geol. Soc.* **134,** 173-184.

679 De la Rocha, C. L., Brzezinski, M. A. and DeNiro, M. J. (2000). A first look at the
680 distribution of the stable isotopes of silicon in natural waters. . *Geochim. Cosmochim.*
681 *Acta* **64**, 2467-2477.

682 DePaolo D. J. (1981) Trace element and isotopic effects of combined wallrock assimilation

683 and fractional crystallization. *Earth Planet. Sci. Lett.* **53,** 189-202.

684 Ding T., Jiang S., Wan D., Li Y., Li J., Song H., Liu Z. and Yao X. (1996) *Silicon Isotope*
685 *Geochemistry.* Geological Publishing House, Beijing, China.

686 Douthitt C. B. (1982) The geochemistry of the stable isotopes of silicon. *Geochim.*
687 *Cosmochim. Acta* **46,** 1449-1458.

688 Ewart, A.J., Chappell, B.W. and Menzies, M.A., 1988. An overview of the geochemical and
689 isotopic characteristics of the eastern Australian Cainozoic volcanic provinces. *J.*
690 *Petrol., Spec. Lithosphere Iss.,* 225-273.

691 Fitoussi C., Bourdon B., Kleine T., Oberli F. and Reynolds B. C. (2009) Si isotope
692 systematics of meteorites and terrestrial peridotites: implications for Mg/Si fractionation
693 in the solar nebula and for Si in the Earth's core. *Earth Planet. Sci. Lett.* **287,** 77-85.

694 Fountain D. M. and Salisbury M. H. (1981) Exposed cross-sections through the continental
695 crust: implications for crustal structure, petrology, and evolution. *Earth Planet. Sci. Lett.*
696 **56,** 263-277.

697 Georg R. B., Reynolds B. C., Frank M. and Halliday A. N. (2006) New sample preparation
698 techniques for the determination of Si isotopic compositions using MC-ICPMS. *Chem.*
699 *Geol.* **235,** 95-104.

700 Georg, R. B., West, A. J., Basu, A. R., Halliday, A.N. (2009a) Silicon fluxes and isotope
701 composition of direct groundwater discharge into the Bay of Bengal and the effect on
702 the global ocean silicon isotope budget. *Earth Planet. Sci. Lett.* **283,** 67-74.

703 Georg R. B., Zhu C., Reynolds B. C. and Halliday A. N. (2009b) Stable silicon isotopes of
704 groundwater, feldspars, and clay coatings in the Navajo Sandstone aquifer, Black Mesa,
705 Arizona, USA. *Geochim. Cosmochim. Acta* **73,** 2229-2241.

706 Grant F. S. (1954) The geological significance of variations in the abundances of the isotopes
707 of silicon in rocks. *Geochim. Cosmochim. Acta* **5,** 225-242.

708 Holbrook W. S., Mooney W. D. and Christensen N. I. (1992) The seismic velocity structure of
709 the deep continental crust. *Continental Lower Crust,* 1-43.

Huang F., Chakraborty P., Lundstrom C. C., Holmden C., Glessner J. J. G., Kieffer S. W. and Lesher C. E. (2010) Isotope fractionation in silicate melts by thermal diffusion. *Nature* **464,** 396-400.

James, D.E. (1981) The combined use of oxygen and radiogenic isotopes as indicators of crustal contamination. *Annu. Rev. Earth Planet. Sci.,* **9**, 311-344.

Kempton P. D. and Harmon R. S. (1992) Oxygen isotope evidence for large-scale hybridization of the lower crust during magmatic underplating. *Geochim. Cosmochim. Acta* **56,** 971-986.

Leeman, W.P., Sisson, V.B. and Reid, M.R. (1992) Boron Geochemistry of the Lower Crust - Evidence from Granulite Terranes and Deep Crustal Xenoliths. *Geochim. Cosmochim. Acta* **56**, 775-788

Liu Y., Gao S., Jin S., Hu S., Sun M., Zhao Z. and Feng J. (2001) Geochemistry of lower crustal xenoliths from Neogene Hannuoba Basalt, North China Craton: Implications for petrogenesis and lower crustal composition. *Geochim. Cosmochim. Acta* **65,** 2589-2604.

Mattey D, Lowry D and Macpherson C (1994) Oxygen isotope composition of mantle peridotite. *Earth Planet. Sci. Lett.* **128 (3-4),** 231-241.

Méheut M., Lazzeri M., Balan E. and Mauri F. (2009) Structural control over equilibrium silicon and oxygen isotopic fractionation: A first-principles density-functional theory study. *Chem. Geol.* **258,** 28-37.

Newton R. C. (1989) Metamorphic fluids in the deep crust. *Ann. Revi. Earth Planet. Sci.* **173,** 85-412.

Opfergelt S., Georg R. B., Delvaux B., Cabidoche Y.-M., Burton K. W. and Halliday A. N. (2012) Silicon isotopes and the tracing of desilication in volcanic soil weathering sequences, Guadeloupe. *Chem. Geol.* **326-327,** 113-122.

Reynolds B. C., Aggarwal J., André L., Baxter D., Beucher C., Brzezinski M. A., Engström E., Georg R. B., Land M., Leng M. J., Opfergelt S., Rodushkin I., Sloane H. J., Van Den Boorn S. H. J. M., Vroon P. Z. and Cardinal D. (2007) An inter-laboratory comparison of Si isotope reference materials. *J. Anal. Atom. Spectrom.* **22,** 561-568.

738 Richter F. M., Davis A. M., DePaolo D. J. and Watson E. B. (2003) Isotope fractionation by
739 chemical diffusion between molten basalt and rhyolite. *Geochim. Cosmochim. Acta* **67,**
740 3905-3923.

741 Richter F. M., Dauphas N. and Teng F-Z. (2009) Non-traditional fractionation of non-
742 traditional isotopes: Evaporation, chemical diffusion and Soret diffusion. *Chem. Geol.*
743 **258,** 92-103.

744 Rudnick R. L. (1990) Nd and Sr isotopic compositions of lower-crustal xenoliths from north
745 Queensland, Australia: Implications for Nd model ages and crustal growth processes.
746 *Chem. Geol.* **83,** 195-208.

747 Rudnick R. L. and Fountain D. M. (1995) Nature and composition of the continental crust: A
748 lower crustal perspective. *Rev. Geophys.* **33,** 267-309.

749 Rudnick R. L. and Taylor S. R. (1987) The composition and petrogenesis of the lower crust:
750 A xenolith study. *J. Geophys. Res.* **92,** 13981-14005.

751 Rudnick R. L. and Taylor S. R. (1991) Petrology and geochemistry of lower crustal xenoliths
752 from northern Queensland and inferences on lower crustal composition. In (Drummond,
753 B., ed) The Australian Lithosphere, *Spec. Pub. Geol. Soc. Australia* **17** 189-208.

754 Rudnick R. L. and Williams I. S. (1987) Dating the lower crust by ion microprobe. *Earth*
755 *Planet. Sci. Lett.* **85,** 145-161.

756 Rudnick R. L. and Goldstein S. L. (1990) The Pb isotopic compositions of lower crustal
757 xenoliths and the evolution of lower crustal Pb. *Earth Planet. Sci. Lett.* **98,** 192-207.

758 Rudnick R. L. and Gao S. (2003) Composition of the continental crust. *Treatise on*
759 *Geochemistry* **3,** 1-64.

760 Rudnick, R.L., McLennan, S.M. and Taylor, S.R. (1985) Large ion lithophile elements in
761 high-pressure granulite facies terrains. *Geochim. Cosmochim. Acta* **49**: 1645-1655.

762 Rudnick R. L., McDonough W. F., McCulloch M. T. and Taylor S. R. (1986) Lower crustal
763 xenoliths from Queensland, Australia: Evidence for deep crustal assimilation and
764 fractionation of continental basalts. *Geochim. Cosmochim. Acta* **50,** 1099-1115.

765 Saal A. E., Rudnick R. L., Ravizza G. E. and Hart S. R. (1998) Re-Os isotope evidence for
766 the composition, formation and age of the lower continental crust. *Nature* **393,** 58-61.

767 Savage P. S., Georg R. B., Armytage R. M. G., Williams H. M. and Halliday A. N. (2010)
768 Silicon isotope homogeneity in the mantle. *Earth Planet. Sci. Lett.* **295,** 139-146.

769 Savage P. S., Georg R. B., Williams H. M., Burton K. W. and Halliday A. N. (2011) Silicon
770 isotope fractionation during magmatic differentiation. *Geochim. Cosmochim. Acta* **75,**
771 6124-6139.

772 Savage P. S., Georg R. B., Williams H. M., Turner S., Halliday A. N., Chappell B. W. (2012a)
773 The silicon isotope composition of granites, *Geochim. Cosmochim. Acta* **92**, 184-202.

774 Savage P. S., Georg R. B., Williams H. M., Halliday A. N (2012b) A silicon isotopic record of
775 long term changes in continental weathering. *Min. Mag.,* **76(6),** 2329.

776 Stähle H. J., Raith M., Hoernes S. and Delfs A. (1987) Element mobility during incipient
777 granulite formation at Kabbaldurga, Southern India. *J. Petrol.* **28,** 803-834.

778 Taylor H. P. and Sheppard S. M. F. Igneous rock: I, Processes of isotopic fractionation and
779 isotope systematics. *Reviews in Mineralogy and Geochemistry*, 1986, **v. 16**, p. 227-271

780 Teng F. -Z., Rudnick R. L., McDonough W. F., Gao S., Tomascak P. B. and Liu Y. (2008)
781 Lithium isotopic composition and concentration of the deep continental crust. *Chem.*
782 *Geol.* **255,** 47-59.

783 Tréguer P., Nelson D. M., Van Bennekom A. J., DeMaster D. J., Leynaert A. and Quéguiner
784 B. (1995) The silica balance in the world ocean: A reestimate. *Science* **268,** 375-379.

785 Van Den Boorn S. H. J. M., Vroon P. Z. and Van Bergen M. J. (2009) Sulfur-induced offsets
786 in MC-ICP-MS silicon-isotope measurements. *J. Anal. At. Spectrom.* **24,** 1111-1114.

787 Villaseca C., Downes H., Pin C. and Barbero L. (1999) Nature and composition of the lower
788 continental crust in Central Spain and the granulite-granite linkage: Inferences from
789 granulitic xenoliths. *J. Petrol.* **40,** 1465-1496.

790 Weyer S. and Schwieters J. (2003) High precision Fe isotope measurements with high mass
791 resolution MC-ICPMS. *Int. J. Mass Spectrom.* **226**, 355-368.

792 Zambardi T. and Poitrasson F. (2011a) A combined Earth-Moon Si isotopes model to track
793 rocks petrogenesis. *Min. Mag.* **75(3),** 2243.

794 Zambardi T. and Poitrasson F. (2011) Precise Determination of Silicon Isotopes in Silicate
795 Rock Reference Materials by MC-ICP-MS. *Geostand. Geoanal. Res.* **35,** 89-99.

796 Ziegler K., Chadwick O. A., Brzezinski M. A. and Kelly E. F. (2005a) Natural variations of
797 δ^{30}Si ratios during progressive basalt weathering, Hawaiian Islands. *Geochim.*
798 *Cosmochim. Acta* **69,** 4597-4610.

799 Ziegler K., Chadwick O. A., White A. F. and Brzezinski M. A. (2005b) δ^{30}Si systematics in a
800 granitic saprolite, Puerto Rico. *Geology* **33,** 817-820.

801 Ziegler K., Young E. D., Schauble E. A. and Wasson J. T. (2010) Metal-silicate silicon
802 isotope fractionation in enstatite meteorites and constraints on Earth's core formation.
803 *Earth Planet. Sci. Lett.* **295,** 487-496.

804 **FIGURE CAPTIONS**

805

806 **Figure 1:** $\delta^{30}Si$ compositions of various volcanic lithologies from Hekla volcano, Iceland, as
807 well as silicate mineral separates, taken from Savage et al. (2011); CPX = clinopyroxene.
808 Also shown is the Si isotope composition of Bulk Silicate Earth, taken from Savage et al.
809 (2010; grey bar is 2sd uncertainty on the average). Data from this study is plotted below the
810 dotted line, separated by protolith lithology – in general, the restite and cumulate material
811 range to lighter $\delta^{30}Si$ values, whereas the felsic melts are isotopically heavy. Error bars are
812 2se.

813

814 **Figure 2:** Graph of $\delta^{30}Si$ versus SiO_2 for the Chudleigh (white symbols) and McBride (grey
815 symbols) xenolith data (error bars are 95% s.e.). Also plotted for comparison is the "igneous
816 array" (crosses and trend line), as defined by Savage et al. (2011). The McBride xenoliths
817 representing melt protoliths fall on or near the igneous trend, and so exhibit a good positive
818 relationship between $\delta^{30}Si$ and SiO_2. The Chudleigh samples do not exhibit this relationship,
819 as they are not representative of equilibrium melt assemblages. Dotted line represents a
820 putative fractional crystallisation trend for the McBride samples, using a bulk D_{Si} of 0.8 and a
821 bulk $\Delta^{30}Si_{solid\text{-}melt}$ of -0.125‰ (tick marks are 10% crystallisation). The dashed line represents
822 the cumulate compositions, calculated by mass balance for each 10% crystallisation step.

823

824 **Figure 3:** Graph of $\delta^{30}Si$ versus $^{87}Sr/^{86}Sr$ and for the Chudleigh and McBride xenoliths
825 (symbols and error bars as for Figure 2). Strontium isotopic data for the McBride samples are
826 age corrected; this correction has not been made for the Chudleigh suite but makes little
827 difference, as Rb/Sr ratios are extremely low; as such, there has been insubstantial ^{87}Sr
828 ingrowth. Dotted lines are AFC trends calculated after DePaolo (1981) for different r values

(cross marks are 10% melt removal steps), starting from a mantle-derived basaltic melt ("B") employing the metasedimentary xenolith as the contaminant (end-member compositions are given in Electronic Annexe EA-1). A line joining "B" to "R" (rhyolite) is analogous to the "igneous array" as plotted in Figure 2, trends parallel to this originating from the r=0.9 AFC curve define magmatic differentiation of an enriched source (fractionating Si without affecting $^{87}Sr/^{86}Sr$).

Figure 4: Graph of $\delta^{30}Si$ versus $\delta^{18}O$ for the Chudleigh and McBride xenoliths (symbols and error bars as for Figure 2; Chudleigh data only shown in (a) for clarity). a) Trend line is for the McBride data only and shows the good relationship between the two isotope systems. Lines are AFC trends calculated after DePaolo (1981) for different r values (cross marks are 10% melt removal steps), starting from a mantle-derived basaltic melt ("B") – in these models, "A" is mafic restite contaminant. Arrow describes the composition of a partial melt forming at f=0.95 of the r=0.9 curve. b) McBride data only, with AFC trends starting from an enriched melt "M", formed as a 30:70 mixture of components "A" and "B". See text for discussion, composition of end-member components are given in Electronic Annexe EA-1.

Figure 5: Graph of $\delta^{30}Si$ versus a) Mg# and b) Eu/Eu* for the Chudleigh and McBride xenoliths (symbols and error bars as for Figure 1). Trend lines in both plots are for the Chudleigh data only.

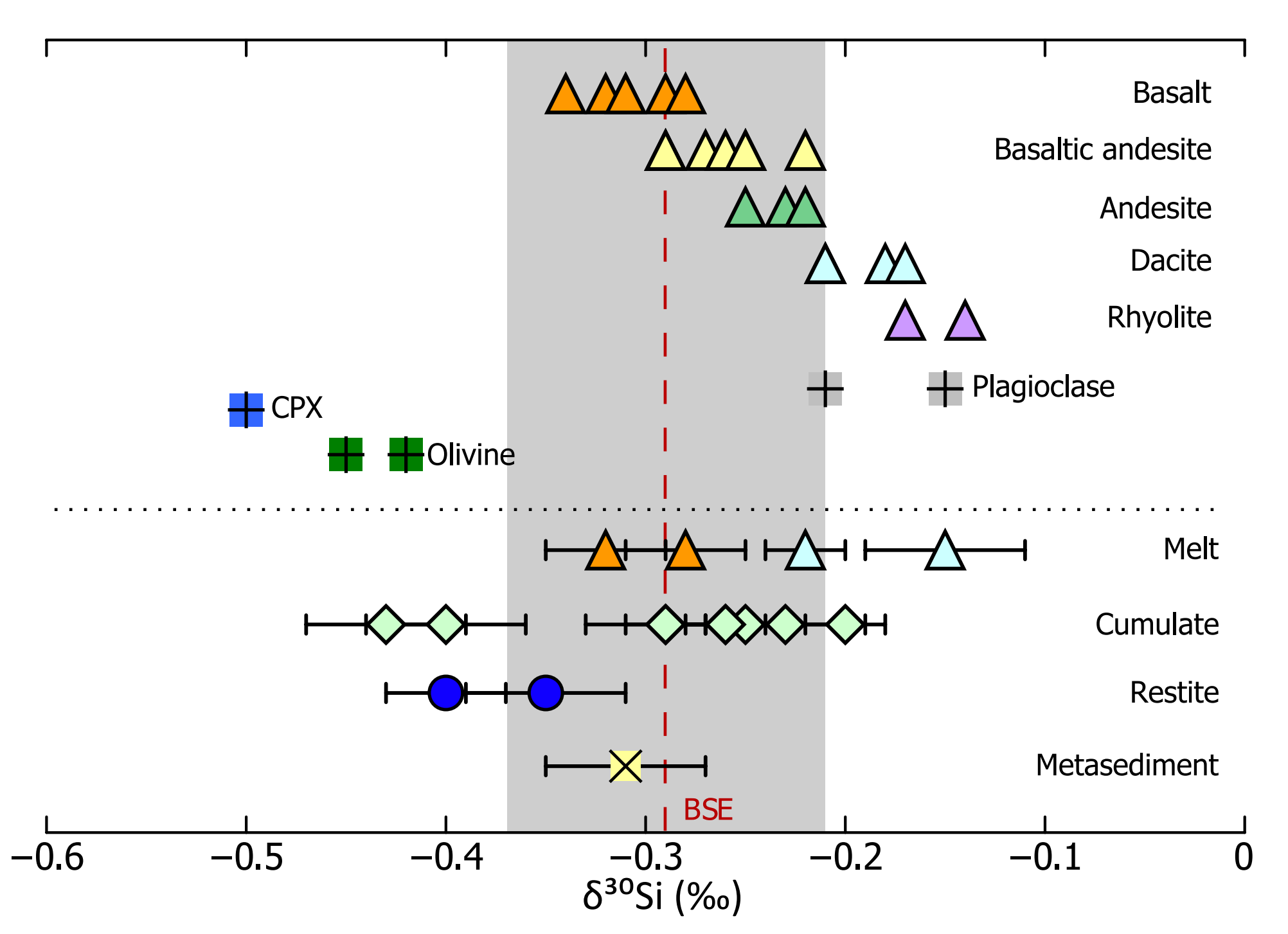
Basalt
Basaltic andesite
Andesite
Dacite
Rhyolite
Plagioclase
CPX
Olivine
Melt
Cumulate
Restite
Metasediment
BSE
−0.6
−0.5
−0.4
−0.3
−0.2
−0.1
0
δ³⁰Si (‰)

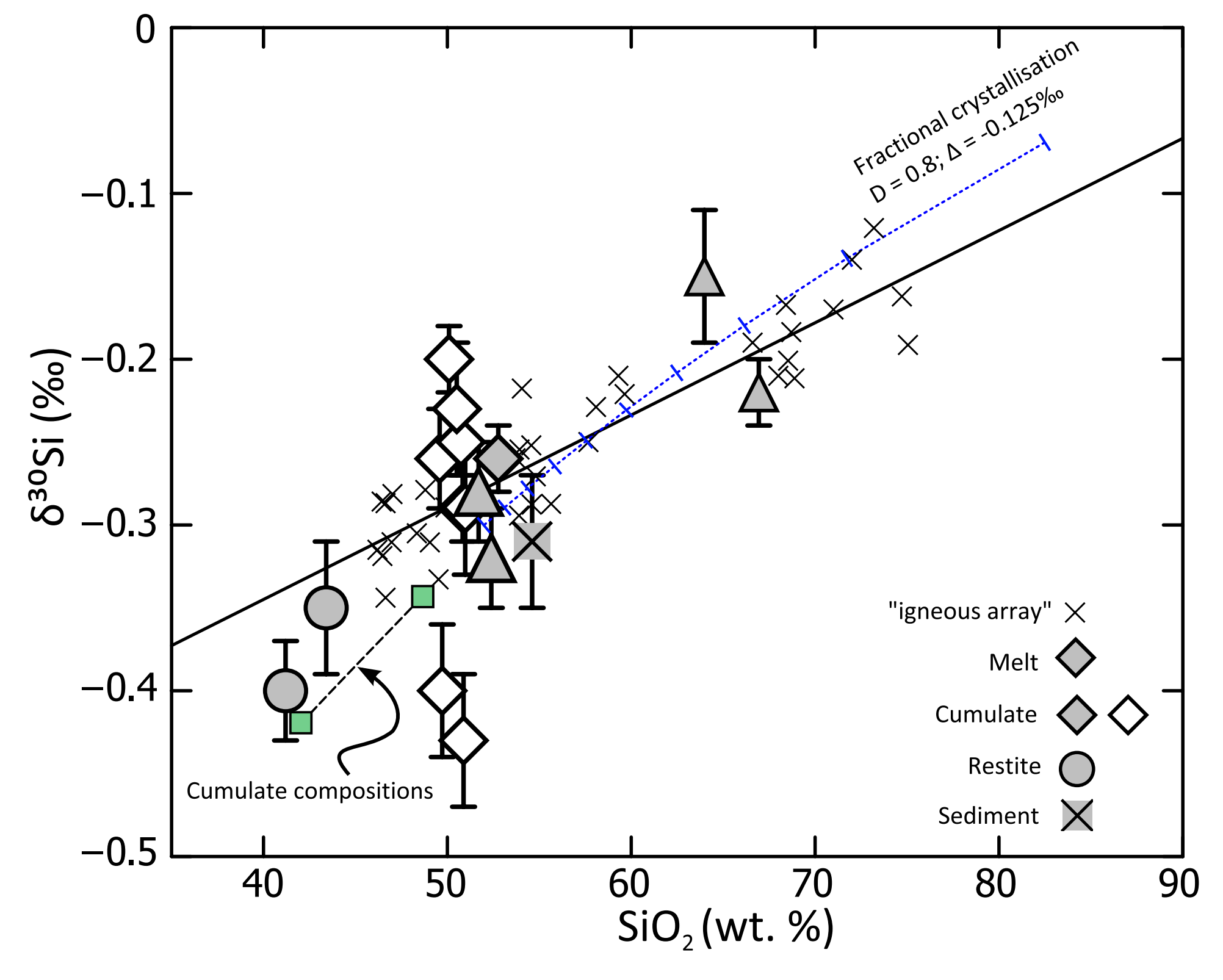
0
−0.1
−0.2
−0.3
−0.4
−0.5
40
50
60
70
80
90
δ30Si (‰)
SiO2 (wt. %)
Fractional crystallisation
D = 0.8; Δ = -0.125‰
"igneous array"
Melt
Cumulate
Restite
Sediment
Cumulate compositions

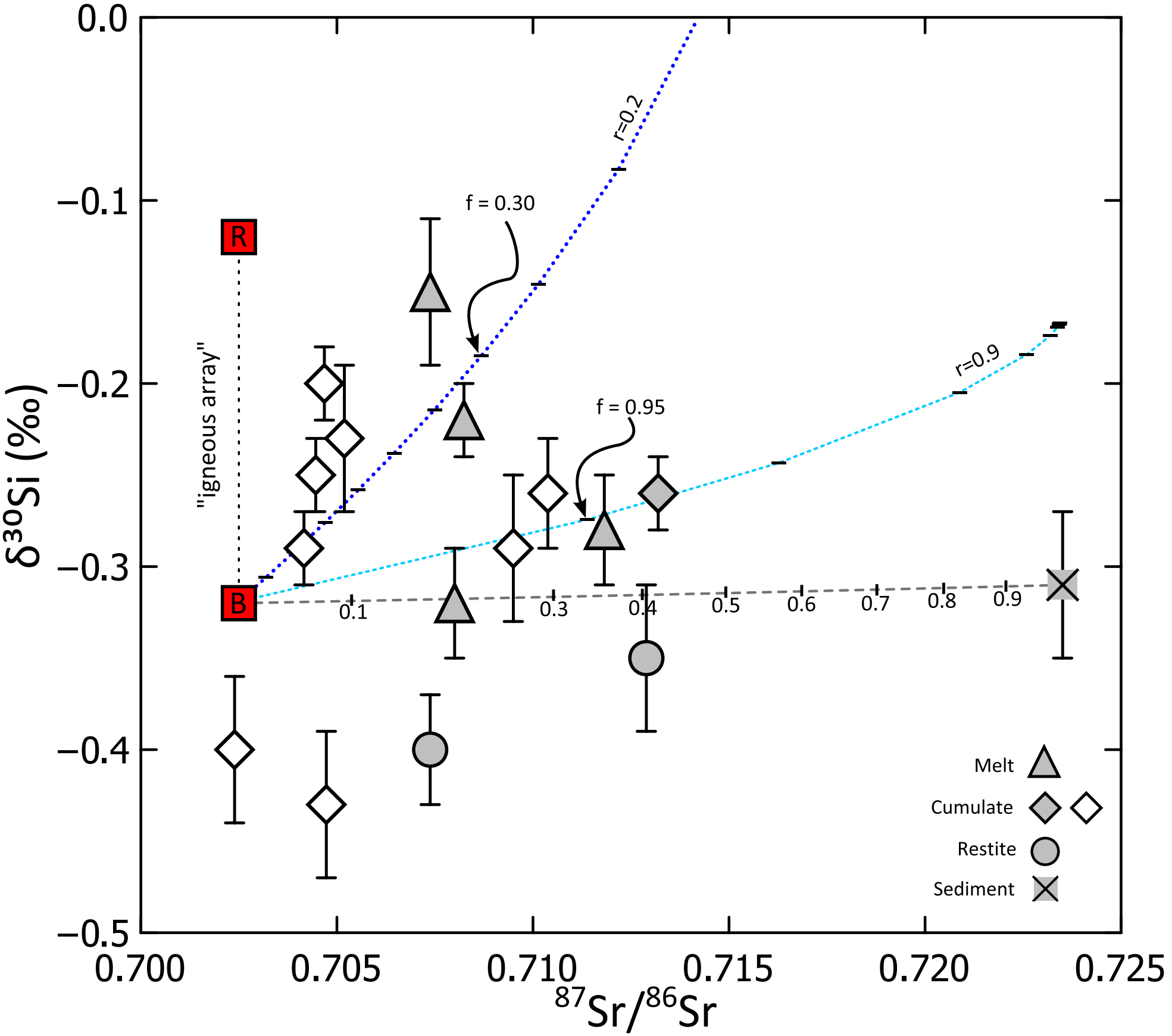
0.0
−0.1
−0.2
−0.3
−0.4
−0.5
δ30Si (‰)
0.700
0.705
0.710
0.715
0.720
0.725
87Sr/86Sr
R
B
"igneous array"
f = 0.30
f = 0.95
r=0.2
r=0.9
0.1
0.3
0.4
0.5
0.6
0.7
0.8
0.9
Melt
Cumulate
Restite
Sediment

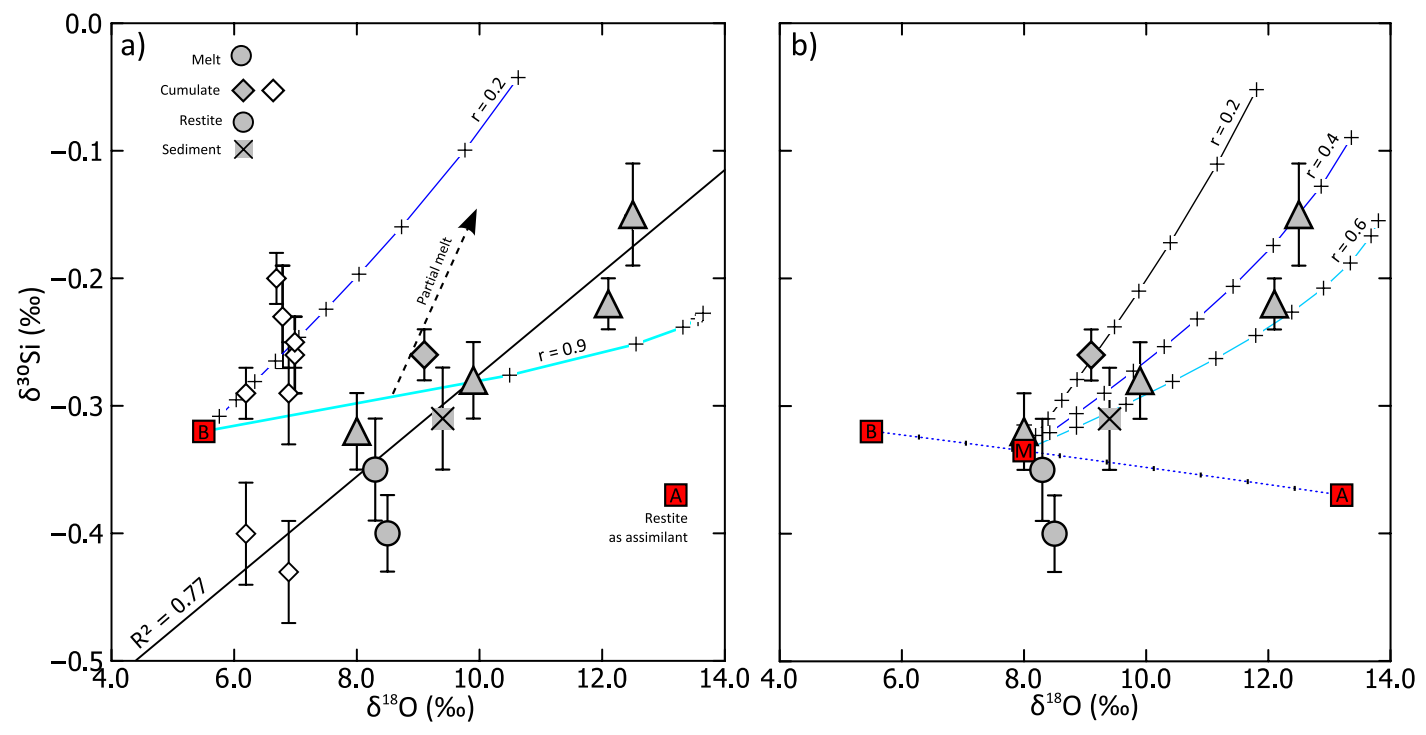
a)
Melt
Cumulate
Restite
Sediment
r = 0.2
Partial melt
r = 0.9
B
A
Restite
as assimilant
R² = 0.77
δ³⁰Si (‰)
δ¹⁸O (‰)
b)
r = 0.2
r = 0.4
r = 0.6
B
M
A
δ¹⁸O (‰)

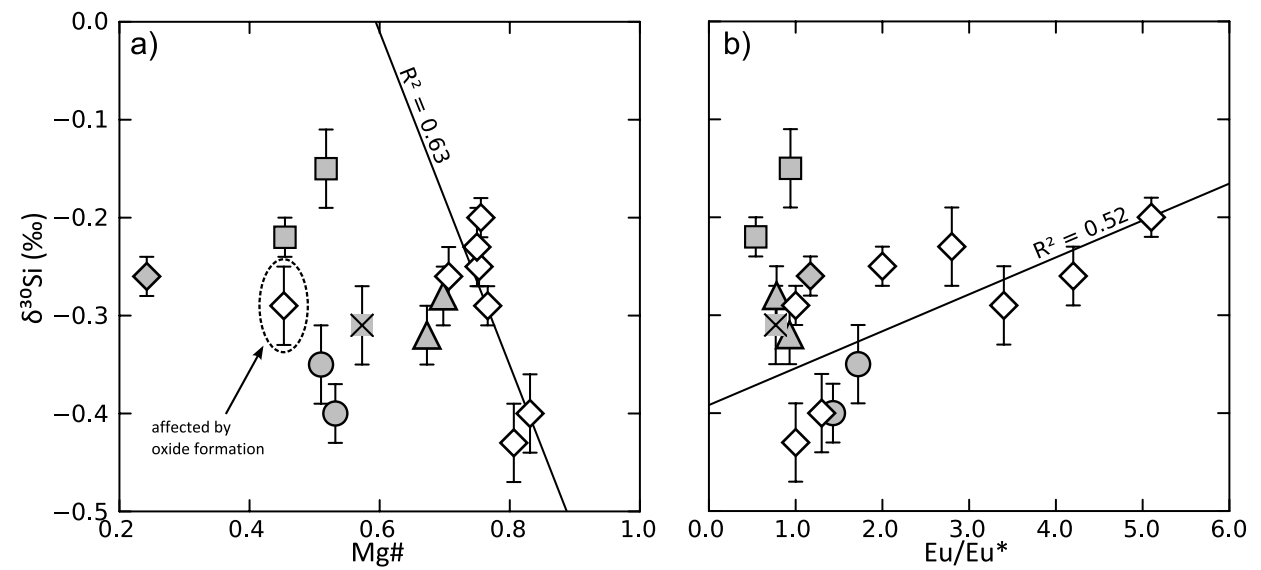
a)
b)
$R^2 = 0.63$
$R^2 = 0.52$
affected by
oxide formation
$\delta^{30}Si$ (‰)
Mg#
Eu/Eu*
0.0
−0.1
−0.2
−0.3
−0.4
−0.5
0.2
0.4
0.6
0.8
1.0
1.0
2.0
3.0
4.0
5.0
6.0

Table 1. Silicon isotope data for external standards and granulite facies xenoliths

Sample	ID	Description	SiO_2 (wt.%)	$\delta^{30}Si$ (‰)	2s.d.	95%s.e.	$\delta^{29}Si$ (‰)	2s.d.	95%s.e.	*n*	$\delta^{30}Si$(m) (‰)	off. (%)
BHVO-2	1			-0.31	0.12	0.04	-0.15	0.08	0.03	11		
	2			-0.29	0.07	0.02	-0.13	0.06	0.02	11		
	3			-0.31	0.05	0.02	-0.15	0.05	0.02	11		
	4			-0.26	0.12	0.04	-0.13	0.09	0.03	11		
	Mean/external reproducibility		49.9	-0.29	0.05		-0.14	0.02		4		
Diatomite	1			1.22	0.11	0.04	0.61	0.08	0.03	11		
	2			1.25	0.11	0.04	0.66	0.12	0.04	11		
	3			1.20	0.10	0.03	0.60	0.06	0.02	11		
	4			1.28	0.12	0.04	0.65	0.07	0.02	11		
	Mean/external reproducibility		100.0	1.24	0.07		0.63	0.06		4		
McBride	83-157	Metasediment	54.6	-0.31	0.13	0.04	-0.15	0.11	0.04	11		
	83-159	Mafic restite	43.4	-0.35	0.12	0.04	-0.17	0.08	0.03	10		
	83-160	Felsic melt	64.0	-0.15	0.13	0.04	-0.07	0.07	0.02	11		
	83-162	Felsic melt	66.9	-0.22	0.06	0.02	-0.14	0.06	0.02	9		
	85-100	Mafic melt	51.7	-0.28	0.09	0.03	-0.13	0.08	0.03	11		
	85-107	Mafic cumulate	52.8	-0.26	0.08	0.03	-0.14	0.08	0.03	11		
	85-114	Mafic restite	41.2	-0.40	0.11	0.04	-0.22	0.04	0.01	11		
	85-120	Mafic melt	52.4	-0.32	0.09	0.03	-0.14	0.05	0.02	11		
Chudleigh	83-107	Plag-rich	49.6	-0.26	0.10	0.03	-0.11	0.05	0.02	11	-0.25	5
	83-110	Pyroxene-rich	50.8	-0.29	0.09	0.03	-0.13	0.07	0.02	11	-0.39	33
	83-112(WR)	Plag-rich	51.0	-0.29	0.11	0.05	-0.13	0.09	0.04	8	-0.24	17
	83-115(WR)	Pyroxene-rich	50.9	-0.43	0.12	0.04	-0.21	0.09	0.03	11	-0.39	9

83-125	Plag-rich	50.7	-0.25	0.06	0.02	-0.12	0.09	0.03	11	-0.28	11
83-127(WR)	Plag-rich	50.1	-0.20	0.08	0.03	-0.11	0.08	0.03	11	-0.26	32
83-131	Plag-rich	50.5	-0.23	0.14	0.05	-0.11	0.09	0.03	11	-0.26	15
BC(WR)	Transitional	49.7	-0.40	0.13	0.04	-0.21	0.13	0.04	11	-0.28	30

Silicon isotope data for external standards and whole-rock xenoliths from McBride and Chudleigh volcanic provinces, Australia. Errors are given as 2 s.d. (2 × standard deviation) and 95% s.e. (95% s.e. = t × s.d./(n)1/2, where t = inverse survival function of the Student's t-test at the 95% significance level and n-1degrees of freedom). Silica contents are taken from Rudnick et al. (1986) and Rudnick and Taylor (1987). The δ^{30}Si(m) values are the predicted Si isotopic compositions of the Chudleigh xenoliths, based on their CIPW normative mineralogy and mineral δ^{30}Si analyses taken from Savage et al. (2011). Also shown are the percentage offsets of the model values from their actual isotopic compositions.

Table 2. Silicon isotopic composition of the deep continental crust

	Mafic	Felsic	Int.	Sed.	δ^{30}Si (‰)	2s.d.
	Proportions (%)					
Lower continental crust						
Simple average[a]					-0.29	0.15
Weighted average[b]					-0.28	0.10
Lithological averages[c]						
Archaean	65	15	15	5	-0.28	0.10
Post-Archaean	70	10	10	10	-0.29	0.11
Extensional regions	40	25	25	10	-0.26	0.13
Shield/platform	90	0	0	10	-0.30	0.10
Middle continental crust						
Weighted average[b]					-0.23	0.15
Lithological average[c]					-0.25	0.15

Estimates of the Si isotopic composition of the lower and middle continental crust, calculated via various methods:

[a]simple arithmetic mean.

[b]weighted mean, using the ratio of a sample's SiO_2 content against the average SiO_2 content of the lower or middle crust (53.4 wt.% and 63.5 wt.%; Rudnick and Gao, 2003) and as the weighting parameter.

[c]calculated by first assigning δ^{30}Si values to crustal lithologies, based on the xenolith data, then combining these values using the range of lithological proportions as inferred by Rudnick and Fountain (1995) – see text for details. A range of isotopic compositions for various crustal composites are given.